Using Sideband Transitions for Two-Qubit Operations
in Superconducting Circuits

P. J. Leek,[1] S. Filipp,[1] P. Maurer,[1] M. Baur,[1] R. Bianchetti,[1] J. M. Fink,[1] M. Göppl,[1] L. Steffen,[1] and A. Wallraff[1]

[1]*Department of Physics, ETH Zurich, CH-8093, Zürich, Switzerland.*
(Dated: December 15, 2008)

We demonstrate time resolved driving of two-photon blue sideband transitions between superconducting qubits and a transmission line resonator. Using the sidebands, we implement a pulse sequence that first entangles one qubit with the resonator, and subsequently distributes the entanglement between two qubits. We show generation of 75% fidelity Bell states by this method. The full density matrix of the two qubit system is extracted using joint measurement and quantum state tomography, and shows close agreement with numerical simulation. The scheme is potentially extendable to a scalable universal gate for quantum computation.

In the pursuit of a scalable architecture for quantum information processing, Josephson-junction based superconducting circuits are currently a leading candidate [1]. Controlled coherent two-qubit interactions, essential for the realization of universal quantum computation, have been demonstrated using a variety of coupling schemes [2–8]. A promising recent advance in the field has been the realization of circuit quantum eletrodynamics (QED) [9] in which superconducting qubits are strongly coupled to single photons in a transmission line resonator. This architecture has been used to couple two qubits over a distance of several millimeters by exchange of a virtual photon between two resonant transmon qubits detuned from the resonator [8] and by exchange of a real photon between two phase qubits in resonance with the resonator [7]. The possibility to achieve such non-local couplings is advantageous for the realization of multi-qubit systems. It is also desirable to be able to switch two-qubit couplings on and off with high accuracy, such that high fidelity operations can be carried out both on individual qubits, and on specifically chosen pairs of qubits, avoiding spurious couplings to other qubits in the system. This issue has been addressed in superconducting circuits by controlling the interaction strength between two qubits via an external parameter [4, 6, 10], or by tuning transitions into and out of resonance [3, 7, 8].

In this Letter we present an experimental realization of a two-qubit coupling scheme in circuit QED that makes use of sideband transitions between the joint qubit and resonator states. In this scheme, qubit transition frequencies may be kept at values chosen for optimal coherence, and do not need to be frequency tuned. Since the coupling is only present when strong microwave drives are turned on to induce the sideband transitions the tunability or on/off ratio of the coupling can be large. The scheme is hence potentially scalable in a similar manner to that achieved with sidebands in trapped ion systems [11, 12].

In the dispersive regime of circuit QED, the qubit transition frequency ω_A is detuned from the resonator frequency ω_r by $\Delta = |\omega_r - \omega_A| \gg g$, where g is the coupling strength between resonator and qubit on resonance (see Fig. 1(a)). Although the qubit and resonator do not directly exchange energy in this case, the residual dispersive coupling still allows sideband transitions linking the qubit and resonator states to be accessed using strong additional microwave drive fields [13, 14]. Blue sideband transitions involve the simultaneous excitation of both qubit and resonator, at a transition frequency $\omega_A^+ = \omega_r + \omega_A$, while the red sideband involves the exchange of an excitation between the two systems, at a transition frequency $\omega_A^- = |\omega_r - \omega_A|$. Such sideband transitions were first observed in a superconducting circuit in an experiment coupling a flux qubit to a superconducting quantum interference device (SQUID) [15].

Due to symmetry considerations in the circuit QED Hamiltonian, single photon sideband transitions with either a Cooper Pair Box (CPB) [16] biased at charge degeneracy, or with a transmon qubit [17, 18], are forbidden to first order. They may however be accessed using two photons, whose sum or difference frequency is equal to one of the sideband transition frequencies $\omega_A^{+/-}$ [14]. A spectroscopic investigation of these two-photon transitions for a CPB has been reported previously, in which two microwave drive fields of different frequency
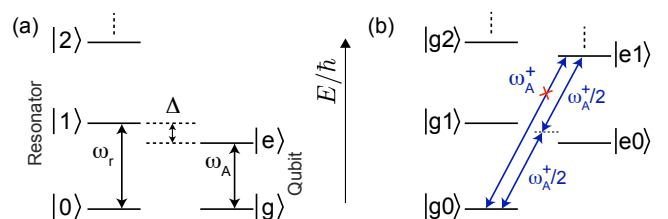

FIG. 1: (a) Schematic of the energy levels of a harmonic oscillator with resonant frequency ω_r, and levels $|n\rangle$ corresponding to photon number n, and qubit with transition frequency ω_A, and ground and first excited states $|g\rangle$ and $|e\rangle$ respectively. (b) Combined level diagram, indicating the blue sideband transition $\omega_A^+ = \omega_r + \omega_A$, which is forbidden to first order, but may be driven using two photons, for example both at a frequency of $\omega_A^+/2$.
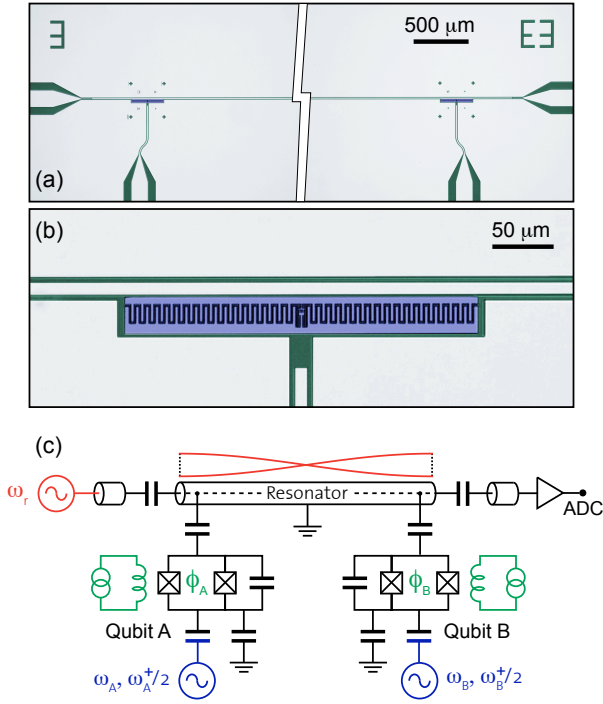
FIG. 2: (a) False color optical microscope image of the two-qubit circuit QED device. The sapphire substrate is shown in dark green, the Niobium resonator in light blue, and the Aluminium qubits in dark blue. (b) High magnification false color optical microscope image of one of the qubits coupled to the transmission line resonator, and a local microwave drive line. (c) Electrical circuit representation of the two-qubit circuit QED device with local controls. The magnetic fluxes Φ_A and Φ_B through the SQUID loops of the qubits are tuned using local superconducting coils (green), while transitions are driven using local microwave drive lines (blue).

were applied to the resonator, detuned slightly from the qubit and resonator frequencies [13]. The increased coupling strength of the transmon to the resonator [17] when compared to the CPB allows driving of the sidebands at larger detunings of the drives from the qubit and resonator. Here we choose to drive the blue sideband with two photons of equal energy, using a single microwave drive of frequency $\omega_A^+/2 = (\omega_r + \omega_A)/2$ (see Fig. 1(b)). In this configuration the drive is equally detuned from the qubit and resonator, maximizing the selectivity of the sideband transition with respect to undesired off-resonant driving of the bare qubit transition and off-resonant population of the resonator.

We work with a two qubit circuit QED device, for which an optical image and circuit schematic are depicted in Fig. 2. A transmon qubit is fabricated at each end of a coplanar waveguide resonator with bare fundamental resonant frequency $\omega_r/2\pi = 6.44$ GHz. The qubits, labelled hereafter as qubit A and B are near identical, with a coupling strength to the resonator $g/2\pi = 133$ MHz and a charging energy $E_C/h = 232$ MHz. The transition fre-

quencies of the qubits are tuned independently by changing the local magnetic fluxes Φ_A and Φ_B through the SQUID loops of qubits A and B respectively, using two small superconducting coils mounted below the chip. Direct qubit and sideband transitions are driven selectively using microwave transmission lines coupled capacitively to each qubit locally (see Fig. 2(c)). For the experiment, the qubits are tuned to transition frequencies of $\omega_A/2\pi = 4.50$ GHz and $\omega_B/2\pi = 4.85$ GHz respectively, well into the dispersive regime.

Sweeping the frequency of a single strong microwave drive on one of the selective qubit drive lines, and simultaneously measuring the resonator transmission to carry out a dispersive measurement of the qubit state [19] shows both the direct qubit transition at ω_A, and an additional spectral line corresponding to the two-photon blue sideband at $\omega_A^+/2$ (see Fig. 3(a)). The high selectivity of the individual qubit drive lines suppresses the coupling to qubit B, the transitions of which are barely visible in Fig. 3(a). The sideband spectral line is shifted down at high drive amplitudes due to the AC-Stark effect on the bare qubit transition [20]. At sufficient drive amplitude, time resolved Rabi oscillations are observed
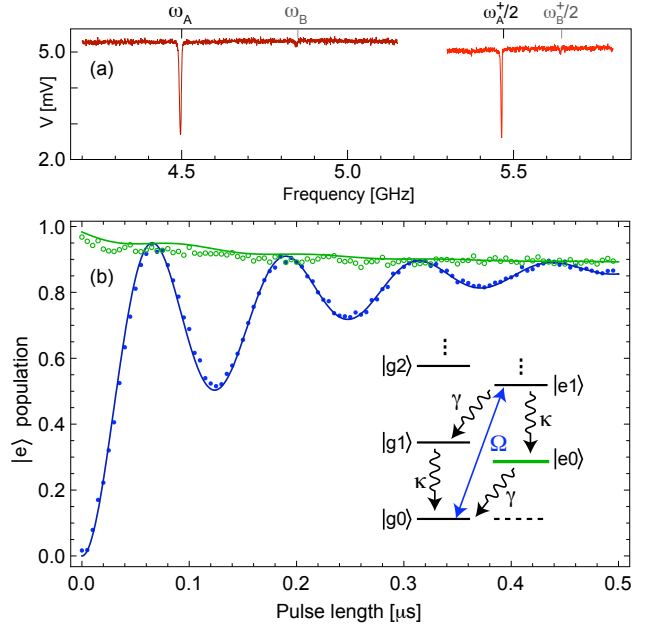

FIG. 3: (a) Spectroscopy on the selective drive line of qubit A, showing the direct transition of the qubit at 4.50 GHz, and the two-photon blue sideband at 5.47 GHz. (b) Time resolved measurements of the excited state population of qubit A as a function of the length of a blue sideband pulse. Blue solid circles show the response for the initial state $|g0\rangle$, and green open circles for $|e0\rangle$. Solid lines: Master equation simulations using decay parameters extracted from separate measurements. (Inset) Level diagram showing competing drive and decay rates in the system.

on the blue sideband transitions (see Fig. 3(b)) by applying microwave pulses of fixed amplitude and varying length, at the Stark-shifted two photon blue sideband frequency, to the local drive line of one qubit. The qubit excited state population is then measured by applying a microwave pulse to the resonator, and comparing the time evolution of the transmission to a numerical solution of the coupled qubit resonator dynamics [21].

Fig. 3(b) shows the extracted excited state population for such an experiment on qubit A (average of 6.6×10^4 repetitions). The solid blue data points show the results obtained when the system is initially in its ground state $|g0\rangle$, while the green open data points correspond to an experiment in which the system is first excited to the state $|e0\rangle$ using a π-pulse on the direct qubit transition. In the latter case, no oscillations are observed since the state $|e0\rangle$ is not addressed by the blue sideband, a fact that was also observed in Ref. 15. Also shown in Fig 3(b) (solid lines) are master equation simulations of the evolution, using values for the qubit relaxation rate $\gamma/2\pi = 0.2$ MHz and photon decay rate $\kappa/2\pi = 1.7$ MHz taken from separate measurements, and with the blue sideband transition rate $\Omega/2\pi = 8.15$ MHz as a fit parameter.

At long times it can be seen in Fig. 3(b) that the qubit excited state population tends to a steady state value of $p_{\rm ss} \approx 0.9$. This can be explained by considering the different drive and decay channels present in the system (see inset). Since the state $|e0\rangle$ has no blue sideband transition, and $\gamma \ll \kappa$, driving the sideband from the ground state $|g0\rangle$ results in a build up of population in $|e0\rangle$. A simple model taking into account only the lowest four levels of the system predicts $p_{\rm ss} = \kappa\Omega/(\kappa\Omega + \gamma\kappa + \gamma\Omega) = 0.87$. It is worth noting that an increase in the ratio κ/γ would allow high fidelity excited state preparation by pumping of the blue sideband, in a similar manner for example to spin preparation by optical pumping in semiconductor quantum dots [22, 23].

Having characterized the sideband Rabi oscillations for both qubits A and B, we implement a sequence of pulses on the two-qubit plus resonator system to generate qubit-qubit entangled states, in a similar manner to that implemented in trapped ions [24]. The full sequence is shown schematically in Fig. 4. At time t_0, the system is in its ground state $|gg0\rangle$, and a resonant π-pulse is first applied to qubit B, generating the state $|ge0\rangle$ at t_1. A $\pi/2$-pulse on the blue sideband of qubit A then generates the entangled state $(|ge0\rangle + e^{i\phi'}|ee1\rangle)/\sqrt{2}$. The qubit-resonator entanglement is then transferred to qubit-qubit entanglement with a π-pulse on the blue sideband of qubit B, generating the Bell state $|\Psi\rangle = (|ge\rangle + e^{i\phi}|eg\rangle)/\sqrt{2}$ at t_3, with the resonator returning to its ground state $|0\rangle$. The phase ϕ of the state is dependent on the phase difference between the two blue sideband pulses in the sequence. An additional resonant π-pulse may now be applied to qubit A to generate the Bell state $|\Phi\rangle = (|gg\rangle + e^{-i\phi}|ee\rangle)/\sqrt{2}$
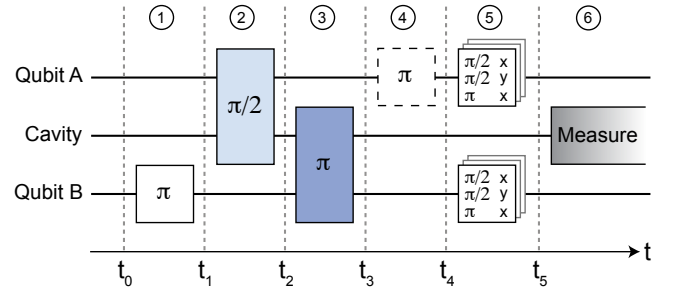

FIG. 4: Pulse sequence implemented on the two-qubit and resonator system, to generate and characterize qubit-qubit Bell states. Direct resonant qubit pulses are shown in white, while blue sideband pulses between resonator and qubits A and B are shown in light and dark blue respectively. The ideal state of the system neglecting decay and imperfections after step i, at each of the intermediate times t_i is indicated in the text.

at t_4.

A full tomographic reconstruction of the two-qubit state is carried out by repeating the pulse sequence 16 times, with different combinations of additional final single qubit rotations (identity, $\pi/2_x$, $\pi/2_y$, and π_x on each qubit). A microwave pulse close to the resonator frequency is then used for an averaged measurement of the two-qubit state. Since the resonator frequency is shifted by a different amount for each of the four two-qubit states $|gg\rangle$, $|ge\rangle$, $|eg\rangle$, $|ee\rangle$ [8], and since the resonator transmission quadrature amplitudes depend non-linearly on this shift, the full density matrix can be parametrised in terms of the 16 averaged measurement results [25]. The closest physical density matrices to those experimentally measured are found using a maximum likelihood approach [26].

Examples of experimental two-qubit density matrices ρ measured after carrying out the pulse sequence for generation of the $|\Psi_+\rangle = (|ge\rangle + |eg\rangle)/\sqrt{2}$ and $|\Phi_+\rangle = (|gg\rangle + |ee\rangle)/\sqrt{2}$ Bell states are shown in Fig. 5(a) and (b). In each case 6.6×10^5 repetitions of the experiment were averaged. The fidelities $\mathcal{F} \equiv (\langle\psi|\rho|\psi\rangle)^{1/2}$ of the measured states ρ with respect to the perfect Bell states $\psi = \Psi_+$ and Φ_+ are $\mathcal{F} = 74\%$ and 76%, respectively, where $\mathcal{F}$ is limited primarily by the resonator photon lifetime, $1/\kappa \approx 100$ ns. We have repeated the state preparation 33 times and calculated the fidelities separately each time, obtaining an average fidelity of $75\pm2\%$ for the full set. The entanglement of formation [27] of the generated states extracted from their density matrices is 0.09 ± 0.04.

Also shown in Fig. 5 ((c) and (d)) are the density matrices resulting from a master equation simulation of the experiment. The simulation makes both the dispersive and rotating wave approximations. Two energy levels for each qubit, and the first 5 levels of the harmonic os-
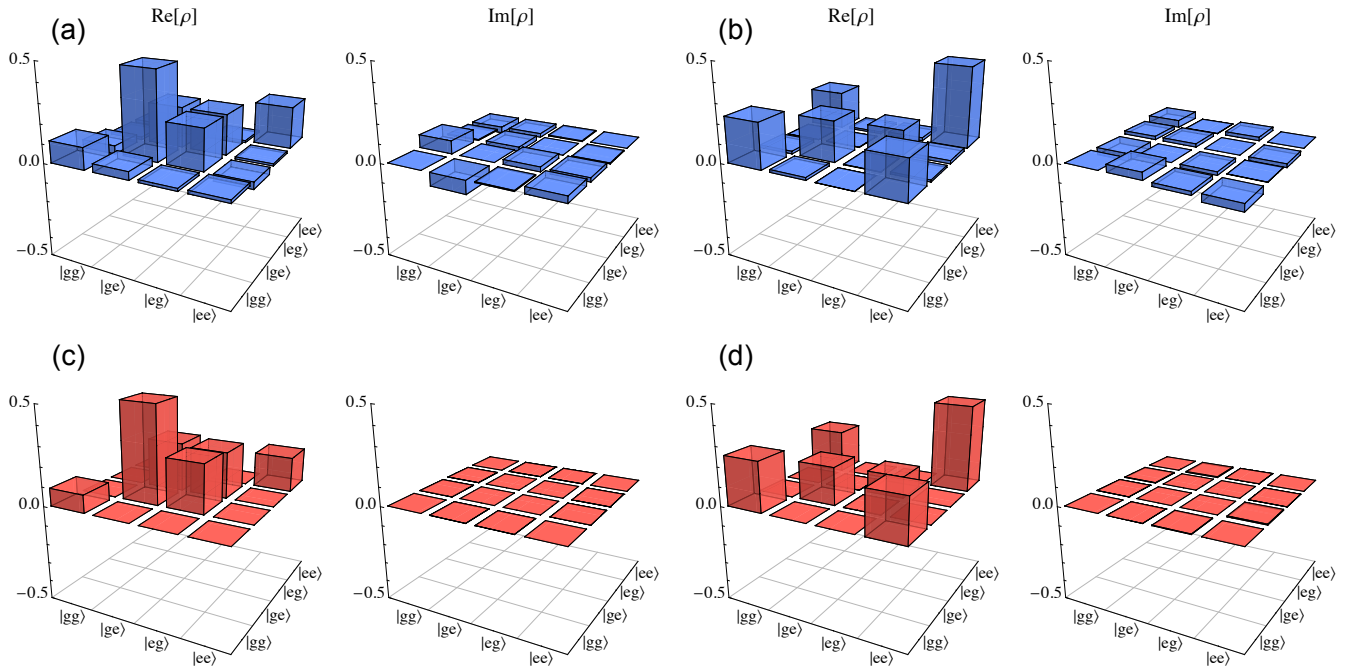
FIG. 5: (a,b) Real and imaginary parts of the two-qubit density matrix extracted from two-qubit tomography measurements after carrying out the pulse sequence to generate the Bell states $|\Psi_+\rangle$ and $|\Phi_+\rangle$ respectively. (c,d) Simulated density matrices corresponding to the states shown in (a) and (b) respectively.

cillator are taken into account. Energy relaxation and decoherence rates for the three individual systems are taken from separate measurements. The fidelity between simulated and measured density matrices is $97 \pm 2\%$, indicating that the loss of fidelity in the experimental state preparation is dominated by photon loss.

The excellent agreement between experiment and simulation gives confidence that with a longer photon lifetime, higher fidelity entangled states are likely to be within reach by this method. The photon lifetime may be increased in future experiments with the use of higher quality factor resonators. The scheme may then be extendable to the implementation of a universal CNOT gate [11, 28], and should scale well to a system with a larger number of qubits. The sidebands may also be used to generate non-classical states of the microwave field in the resonator, such as Fock states.

---

[1] J. Clarke and F. K. Wilhelm, Nature (London) **453**, 1031 (2008).

[2] T. Yamamoto *et al.*, Nature (London) **425**, 941 (2003).
[3] M. Steffen *et al.*, Science **313**, 1423 (2006).
[4] T. Hime *et al.*, Science **314**, 1427 (2006).
[5] J. H. Plantenberg *et al.*, Nature (London) **447**, 836 (2007).
[6] A. O. Niskanen *et al.*, Science **316**, 723 (2007).
[7] M. A. Sillanpää *et al.*, Nature (London) **449**, 438 (2007).
[8] J. Majer *et al.*, Nature (London) **449**, 443 (2007).
[9] A. Wallraff *et al.*, Nature (London) **431**, 162 (2004).
[10] S. H. W. van den Ploeg *et al.*, Phys. Rev. Lett. **98**, 057004 (2007).
[11] F. Schmidt-Kaler *et al.*, Nature (London) **422**, 408 (2003).
[12] H. Häffner *et al.*, Nature (London) **438**, 643 (2005).
[13] A. Wallraff *et al.*, Phys. Rev. Lett. **99**, 050501 (2007).
[14] A. Blais *et al.*, Phys. Rev. A **75**, 032329 (2007).
[15] I. Chiorescu *et al.*, Nature (London) **431**, 159 (2004).
[16] V. Bouchiat *et al.*, Physica Scripta **T76**, 165 (1998).
[17] J. Koch *et al.*, Phys. Rev. A **76**, 042319 (2007).
[18] J. Schreier *et al.*, Phys. Rev. B **77**, 180502(R) (2008).
[19] A. Wallraff *et al.*, Phys. Rev. Lett. **95**, 060501 (2005).
[20] D. I. Schuster *et al.*, Phys. Rev. Lett. **94**, 123602 (2005).
[21] A. Blais *et al.*, Phys. Rev. A **68**, 062320 (2004).
[22] M. Atature *et al.*, Science **312**, 551 (2006).
[23] B. D. Gerardot *et al.*, Nature (London) **451**, 441 (2008).
[24] C. F. Roos *et al.*, Phys. Rev. Lett. **92**, 220402 (2004).
[25] S. Filipp *et al.*, arXiv:0812.2485 (2008).
[26] M. G. A. Paris and J. Rehácek (Eds.), *Quantum State Estimation* (Springer, Berlin, 2004).
[27] C. H. Bennett *et al.*, Phys. Rev. A **54**, 3824 (1996).
[28] M. Riebe *et al.*, Phys. Rev. Lett. **97**, 220407 (2006).